Investigating the Influence of the Spacer Length on Anion-Exchange Membrane Properties Using a Reactive Molecular Model

Thibaut Flottat, Benoit Latour, Florent Goujon, Patrice Hauret, Patrice Malfreyt

Investigating the Influence of the Spacer Length on Anion Exchange Membranes Properties using a Reactive Molecular Model.

Thibaut Flottat,*,†,‡ Benoit Latour,‡ Florent Goujon,† Patrice Hauret,‡ and Patrice Malfreyt*,†

†*Université Clermont Auvergne, CNRS, Clermont Auvergne INP, Institut de Chimie de Clermont-Ferrand, F-63000 Clermont-Ferrand, France*
‡*Manufacture Française des Pneumatiques Michelin, 23 Place des Carmes, Clermont-Ferrand, 63040, France*

E-mail: Thibaut.Flottat@michelin.com; Patrice.Malfreyt@uca.fr

Abstract

This study investigates the influence of spacer length within anion exchange membranes (AEMs) on their diffusion properties. Using reactive molecular dynamics with ReaxFF, three polyphenylene oxide (PPO) based AEMs functionalized with trimethylamine (TMA) cationic groups at two hydration levels ($\lambda = 10$ and 20) have been simulated at the molecular scale through three alkyl spacer chains lengths : methyl (PPO1-TMA), pentyl (PPO5-TMA) and decyl (PPO10-TMA). Our simulations capture the nanophase separation due to the amphiphilic nature of simulated materials, where water channel emerges to enable OH^- transport through Grotthuss and classical mechanisms. We find that the number of hydrogen bonds formed between OH^- and H_2O molecules is a key-parameter governing diffusion properties of OH^-. At the lower hydration level, PPO1-TMA has the lowest diffusion properties, whereas PPO5 and PPO10-TMA membranes show the same diffusion, because pentyl and decyl spacers bend and remain stuck on the backbone because of their hydrophobicity. At the higher hydration level, the three membranes exhibit identical diffusion properties, irrespective of their spacer length, as OH^- molecule approaches its bulk-like behaviour.

1 Introduction

Fuel cells (FCs), which aim to convert chemical energy of a fuel to electric energy, have been considered as an alternative to the use of fossil fuels in the context of environmental pollution, greenhouse gas emission and a sustainable future.[1–3] FCs[1] are able to provide electricity with zero emission, high energy conversion and to release water when hydrogen is used as the fuel. Actually, there are several kinds of FCs[1,4,5] distinguished by the nature of the electrolyte. Alkali fuel cells (AKFCs) use generally a solution of potassium hydroxide as the liquid electrolyte whereas a phosphoric acid solution constitutes the electrolyte in phosphoric acid fuel cells (PAFCs). Molten carbonate fuel cells (MCFs) use an electrolyte composed of a molten carbonate salt mixture whereas solid oxide fuel cells (SOFCs) have solid oxide or ceramic electrolytes. As the electrolyte layer is formed by a polymer membrane, the fuel cell is known as polymer electrolyte membrane fuel cell (PEFC). In anion exchange membrane fuel cells (AEMFCs), the polymer enables the conduction of hydroxide anion whereas in proton exchange membrane fuel cells (PEMFCs), the

polymer membrane is designed to conduct H^+ protons.

In these last years, considerable activity of research has been devoted to improving the performance of polymer electrolyte fuel cells due to high expectations in the field of powering automobiles.[6] However, manufacturing costs are the main factor that limits their worldwide commercialization.[7,8] As a result, anion exchange membranes (AEMs) have been the source of more and more attention since they offer new options in terms of electrochemical kinetics of the oxygen reduction reaction in alkaline media, use of non-precious metal electrocatalysts, choice of fuels and minimization of the corrosion problems in the alkaline environment.[2,9,10]

In contrast to PEMFCs, AEMFCs operate in alkaline conditions and oxygen reduction gives OH^- ions at the cathode that are transported through a solid PEM to the anode. The hydroxide anions react then with the fuel to produce water and electrons. One of the greatest challenges for this technology[11] concern the development of new AEMs that combine high hydroxide conductivity with a long-term chemical stability in alkaline conditions. However, AEMs show lower ionic conductivity as compared to the reference Nafion PEM due to the intrinsic lower mobility of OH^- ions. Additionally, AEMs are likely to absorb CO_2 from the ambient air and form bicarbonate and carbonate ions reducing then the ionic conductivity[12] and affecting the performance. As a result, the challenge consists of designing AEMs that perform in ion-exchange capacity, OH^- conductivity, chemical and mechanical stabilities while providing a suitable water uptake[13,14] and a moderate swelling ratio.[15]

AEM is typically composed of a polymer backbone onto which fixed cationic sites are tethered. A variety of polymers[2,5,16–18] such as poly(vinyl alcohol) (PVA), poly(ether ether ketone) (PEEK), poly(ether ether ketone ketone) (PEEKK), poly(tetrafluoroethylene) (PTFE), poly(2,6-dimethyl-1,4-phenyleneoxide) (PPO) and many others have been proposed to design AEMs. These polymers have been functionnalized with various cationic groups such as quaternary ammonium, tertiary diamines, guanidinium, and pyridinium.[19–22] Quaternary ammonium (QAs) are the most popular due to their promising ionic conductivity and ease of synthesis[15] and PPO polymers opens up numerous opportunities for the development of AEMs with targeted properties.[23] PPO also shows good mechanical properties, high chemical and thermal stability in alkaline conditions.

An increasing ionic conductivity can be improved by favoring the hydrophilic/hydrophobic microphase separation. By playing on the hydrophobic parts, it is possible to build larger ionic clusters which are at the origin of the formation of interconnected ionic channels and which help the ionic transportation. The structures of the polymer backbone and the cationic headgroups as well as their interactions are critical to form AEM microphase.[5,15] Instead of attaching QA groups in benzylic positions on the PPO polymer backbone, previous works[24,25] have shown that it is possible to attach them via an alkyl spacer chain leading to a high local mobility of the cationic groups. The resulting AEM shows an efficient phase separation and enhanced ionic conductivity. The side-chain functionality has also been investigated to achieve highly conductive AEMs.[17] The impact of crosslinking and nature of the crosslinkers were studied on the physicochemical, morphological and electrochemical properties of the crosslinked PPO membranes.[26]

In addition to design and synthesis, the characterization of the AEMs was carried out mainly from an experimental point of view by using various techniques including, but not limited to, UV-visible spectroscopy, X-ray powder diffraction, Fourier-transform infrared spectroscopy, small angle X-ray scattering, NMR spectroscopy, and thermogravimetric analysis, conductivity measurements and tensile tests.[6,9,18,23–25] Given the challenges posed by AEMs in terms of synthesis, characterization, in-depth understanding of the structure-properties relationships, ionic transport, hydration, formation of ionic channels it is clear that molecular simulation[27] can be a powerful and essential technique. However, the diversity of length and time scales underlying the properties of AEMs raises the question of the compu-

tational effort and therefore the choice of the most adapted method for calculating the property.[11,14,28–39] It is impossible for a single simulation method to cover the entire spectrum of spatial and temporal scales. For instance, if we are interested in investigating the segregation in polymer membranes, the most suitable strategy is to combine the use of coarse-grained models[29,30,40] with genuine mesoscopic simulations techniques.[31,33,37,38,41–43] Simulations with molecular descriptions were used to investigate the transport of OH^- trough the vehicular diffusion[44] and the impact of the hydration state on the structure at the nanoscale.[32,39,45] If the aim is to tackle the diffusion process through the Grotthuss hopping mechanism[46] or phenomena such chemical stability and degradation that can lead to bond breaking and bond formation, it is then required to replace the non-reactive force field used in non-reactive molecular dynamics (MD) by a reactive model. Even if other simulation methods such as *ab initio* MD (AIMD),[47] hybrid quantum mechanics / molecular mechanics (QM/MM),[48,49] charged-optimized many-body (COMB) potential[50] are able to consider chemical reactions but only for small system-sizes, the use of the reactive force field (ReaxFF) remains a promising route for studying Grotthuss mechanism of hydroxyl groups in membranes since this model is much faster than quantum calculations. A very promising methodology[51] consisting in designing a machine learned force field has been successfully applied to an perfluorinated ionomer, Nafion, in order to investigate the structural and proton transition transport properties in various humidified conditions.

Actually, the ReaxFF force field,[52] firstly proposed by Van Duin et al. in 2001 for hydrocarbon systems[53,54] has been extended to various systems and properties[55–61] along with different reparametrizations.[34,62–64] MD simulations associated with the ReaxFF force field were performed to investigate the diffusion of hydroxide anions and water molecules for three functionalized PPO-trimethylamine, PPO-dimethylbutylamine and PPO-dimethyloctylamine.[28] Another reactive simulation[36] was carried out on a PPO-polymer functionalized with two different structures of QA groups in order to investigate the contributions of vehicular and Grotthuss mechanisms in hydroxide motion. Material designers have several levers at their disposal to tune conduction properties, including spacer length, steric hindrance and/or chemical nature of the cationic group and ion exchange capacity (IEC). It is then possible to monitor and control the role of these levers on a molecular scale by developing simulations on this scale. In this work, we propose to study the transport properties of diffusive species, namely water molecules and hydroxide ions in PPO functionalized with QA containing alkyl chains by applying reactive molecular dynamics simulations. We focus on the impact of the number of spacer units in-between the QA group and the polymer backbone on the transport of hydroxide anions in PPO-TMA AEMs.

The paper is organized as follows. Section 2 contains the composition of the simulated AEMs, the description of the molecular model. The results and discussions are provided in Section 3. We conclude this work in Section 4.

2 Computational procedures and methodology

2.1 Description of the systems

Three hydrated functionalized polyphenylene oxide (PPO) based AEMs and a bulk KOH solution were modeled. Spacers are made of alkyl chains ended with trimethylamine (TMA) cationic groups. Three spacer lengths ranging from methyl-TMA to decyl-TMA including pentyl-TMA were chosen. For clarity, we will denote the shorter spacer length PPO1-TMA, the intermediate spacer length PPO5-TMA and the longer spacer length PPO10-TMA. The chemical structures are represented in Figure 1. H atoms were added at the end of polymer chains, x was set equal to 1 and y equal to 3 for all membranes leading to equivalent weight (EW) of 540, 595 and 665 $\mathrm{g\,mol^{-1}}$ for PPO1-TMA, PPO5-TMA, PPO10-TMA, respectively. EWs correspond to the dry polymer molecular

mass divided by the number of cationic groups. Those values match experimental systems studied in Ref. 65 (PPO1-TMA and PPO5-TMA only) whose Ion Exchange Capacity (IEC where IEC = 1000/EW) are approximately equal to 1.67 (PPO1-TMA) and 1.90 (PPO5-TMA).

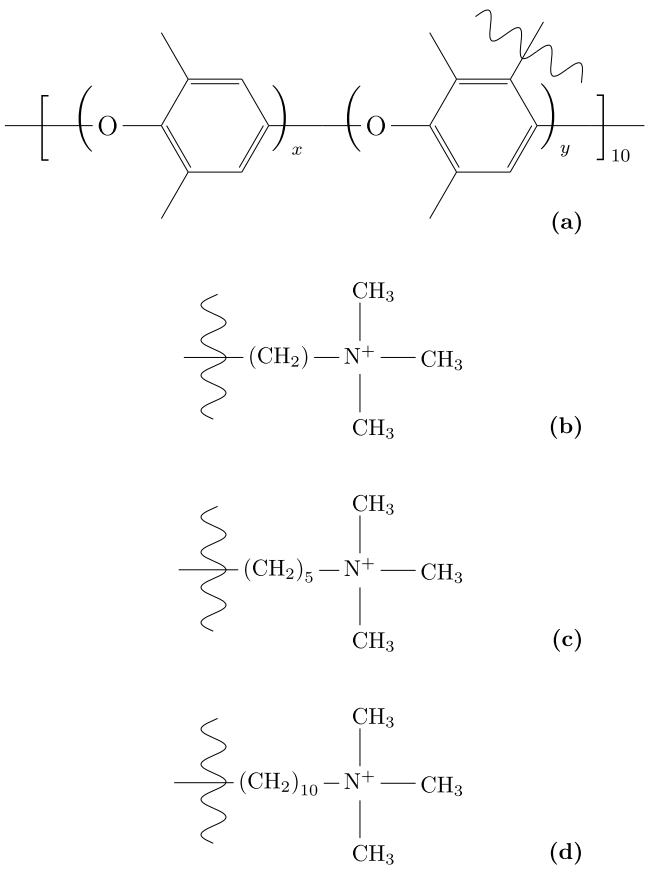

Figure 1: a) Molecular structures of the simulated PPO polymer unit and of the QA groups formed by b) a carbon chain methyl, c) a pentyl chain and d) a decyl chain and ended with a TMA group.

Each simulation box was built with a random morphology using the *Amorphous Builder* of *MedeA* software[66] with 25 polymer chains. Two hydration levels, described by the parameter λ, were chosen: 10 and 20. λ is the number of water molecules per hydroxide ions, i.e. $\lambda = n_{H_2O}/n_{OH^-}$. These hydration levels are typically observed in PPOs tethered with flexible cationic alkyl side chains with different combinations of spacer units and extender chains.[24,25] We simulated these systems at room temperature under the same conditions as the previous reactive molecular simulations.[28,36,62] KOH solutions were also modeled. This allows us to study more precisely the impact of confinement induced by the polymer host matrix on diffusive species, *i.e.*, OH^- ions. Those reference systems were built to match the number of water and OH^- molecules, and K^+ ions were used as counter ions. In what follows, free OH^- corresponds to a KOH solution. The summary of simulation boxes is presented in the Table 1. Five independent simulation boxes were created for each system and each hydration level in order to estimate the statistical fluctuations of simulated properties. Table 1 also emphasizes that the system-sizes of AEMs investigated in this work in terms of number of chains, chain length and corresponding number of hydroxide ions and water molecules are much larger than those studied by previous reactive molecular dynamics simulations.[28,36,62] Size effects in these heterogeneous systems are thus expected to be weakened.

Table 1: Description of simulated systems in terms of number of molecules and atoms in the simulation box where $n_{\mathbf{chains}}$, $n_{\mathbf{OH^-}}$, $n_{\mathbf{H_2O}}$, $n_{\mathbf{atoms}}$ refer to the number of polymer chains, hydroxide ions, water molecules and atoms in the simulation cell, respectively.

λ	n_{chains}	n_{OH^-}	n_{H_2O}	n_{atoms}
PPO1-TMA				
10	25	250	2500	28050
20	25	250	5000	35550
PPO5-TMA				
10	25	250	2500	31050
20	25	250	5000	38550
PPO10-TMA				
10	25	250	2500	34800
20	25	250	5000	42300
Free OH^-				
10		250	2500	8000
20		250	5000	15500

2.2 Non-reactive molecular dynamics

Before starting reactive MD simulations, non-reactive MD simulations were performed to generate relaxed systems which will then be simulated with the reactive force field. Indeed, this option is faster than a full reactive relaxation protocol because reactive MD is more time consuming than non-reactive MD. Moreover, unwanted reactions such as degradation of AEMs[67] could happen during high temperature steps if only reactive MD was used. Systems were first modeled using the Polymer Consistent Force Field-enhanced ($PCFF_+$), which is an enhanced version of PCFF developed by *MedeA* software.[66] It mostly contains additional impropers and torsional terms in order to accurately describe properties and geometries of organic molecules. In order to control temperature and pressure, the Nosé-Hoover thermostat and barostat[68,69] were used with a damping factor of $100\,\delta t$ for the thermostat and $1000\,\delta t$ for the barostat. The cutoff radius was fixed to 12 Å. Coulombic interactions were handled using PPPM solver[70] with a precision of 10^{-6}. Equations of motion were integrated using the standard velocity-Verlet algorithm, and periodic boundary conditions were applied in the three directions of space. Non-reactive MD simulations were conducted with the LAMMPS software.[71]

To generate the initial configurations for reactive MD, we used the same relaxation protocol as in our previous study.[39] This relaxation scheme is based on the one used by Gilois et al. in Ref. 72, based itself on a protocol described in Ref. 73. The protocol is described in Section 1 of the Supporting Information. CH bonds of AEMs, OH bonds of water and hydroxide ions and HOH angles of water were constrained using SHAKE algorithm.[74]

2.3 Reactive molecular dynamics

Introduced in 2001 by Van Duin et al.,[53] ReaxFF is a new class of reactive force fields, based on the concept of bond orders. Introducing a dependence between bond orders and intramolecular part of the potential enables bond breaking and bond formation. The readers are directed to Refs. 53,54 that fully describe potential energy expressions of ReaxFF.

The PPO-based AEMs were modeled by using the CHON2017_weak force field.[34] This force field has been parameterized from the protein-2013 model[75] to describe accurately weak interaction of functionalized hydrocarbon/water molecules and has already been used in reactive MD studies on PPO-based AEMs.[28,36]

Starting from the last frame of non-reactive MD runs, a 0 K minimization step was performed, followed by a 200 ps run in the NpT ensemble at 1 bar and 298.15 K to equilibrate density since the $PCFF_+$ model underestimates this property. Following that, a 1200 ps trajectory in the NVT ensemble at 298.15 K was acquired, the last 1000 ps used for data analysis. The ReaxFF simulations were conducted with the AMS 2021 software[76] using a 0.25 fs time-step. The Berendsen thermostat was used with a damping factor of $100\,\delta t$. Tapered bond orders[77] and Furman torsions[78] were applied. Figure 2 shows a snapshot of a final configuration of PPO10-TMA at $\lambda = 10$ in which a nanophase segregation can be observed with a well-connected and percolated water network.

3 Results and discussion

Conductivity stands out as a crucial factor for gauging the efficiency of a fuel cell. This property is directly related to hydroxide ions diffusion processes. Such processes can be captured by experiments[79] and also by numerical methods allowing chemical reactions. As we discussed in our previous study,[39] the first parameter governing diffusion properties is the percolation state of the water network, depicted by the mean percolation probability M which quantifies how water molecules are connected to their images trough periodic boundary conditions. The mean percolation probability M is

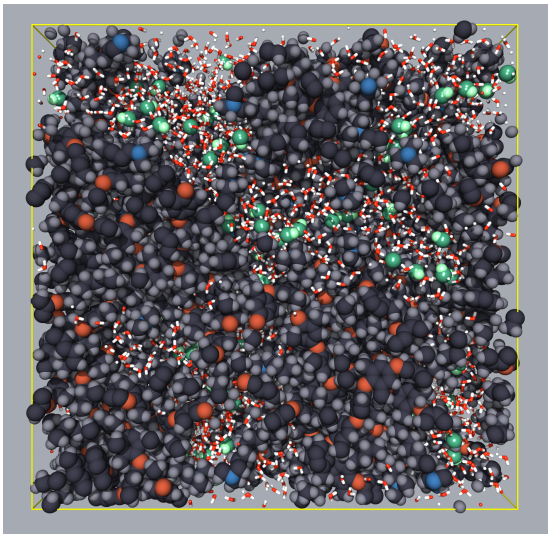

Figure 2: Snapshot of a final configuration of PPO10-TMA for $\lambda = 10$. Polymer atoms are display in spacefill and dark colors, hydroxide ions are represented in green while water molecules are represented as smaller ticks.

defined as

$$M = \frac{1}{3L_\lambda} \sum_{\Delta} \sum_{c} \mathcal{H}_{\Delta,c}\, l_c, \qquad (1)$$

where the first sum is carried out over $\Delta = \{x, y, z\}$, the three directions of space and the second one over clusters of water molecules and OH^- anions. The reader is redirected to ref. 39 for further details about graph theory used in this analysis. $\mathcal{H}_{\Delta,c}$ is the Heaviside function which is equal to 1 if a node of the cluster is connected to its image trough periodic boundaries in the considered direction, 0 otherwise. l_c is the number of nodes in the cluster c. The mean percolation probability is plotted on Figure 3. The percolation state of the water network is identical to the three membranes at any hydration level indicating that the water network structure is therefore independent of the spacer length. A value of ≈ 0.7 (respectively ≈ 0.9) indicates that 70% (resp. 90 %) of the water phase network is percolated at $\lambda = 10$ (resp. $\lambda = 20$). As a result, the differences in properties reported in this study cannot be related to the adopted water network structure at a given hydration level. For completeness, the distribution of water and hydroxide around the TMA^+ group is illustrated by spatial distribution functions in Figure S1 of the Supporting Information.

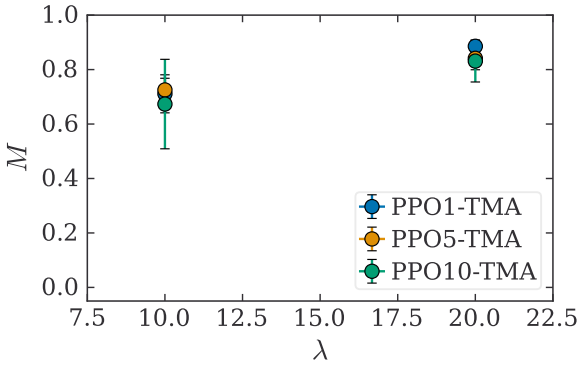

Figure 3: Mean percolation probability M as a function of λ for the three membranes. If not visible, error bars are smaller than symbols.

As a consequence, the starting point of the discussion will be the analysis of the mean square displacements (MSDs) of water molecules (Figure 4) and hydroxide ions (Figure 5). MSDs were computed using equation given in Section 3 of the Supporting Information. To compute MSD of reactive species, their trajectories must be regenerated. Indeed, systems topology is not fixed in reactive molecular dynamics with respect to non-reactive molecular dynamics. Only the number of species is conserved. The methodology for regenerating OH^- ions trajectory is described in Section 4 of Supporting Information.

Considering only vehicular mechanism, MSDs are identical at any hydration level for all membranes (see Figure 4). At $\lambda = 10$, Figure 4a shows that the MSD of hydroxide ions for PPO5-TMA and PPO10-TMA membranes are identical and higher than PPO1-TMA whereas at $\lambda = 20$, MSDs of all membranes are rather similar (see Figure 4b). Diffusion coefficients calculated from MSDs curves and reported in Table 2 consider both vehicular and Grotthuss mechanisms. These coefficients are of the same order of magnitude as those of previous reported studies.[28,36,62] Differences might come from finite size effects since systems simulated in this study are larger. The impact of the confinement induced by the polymer host matrix

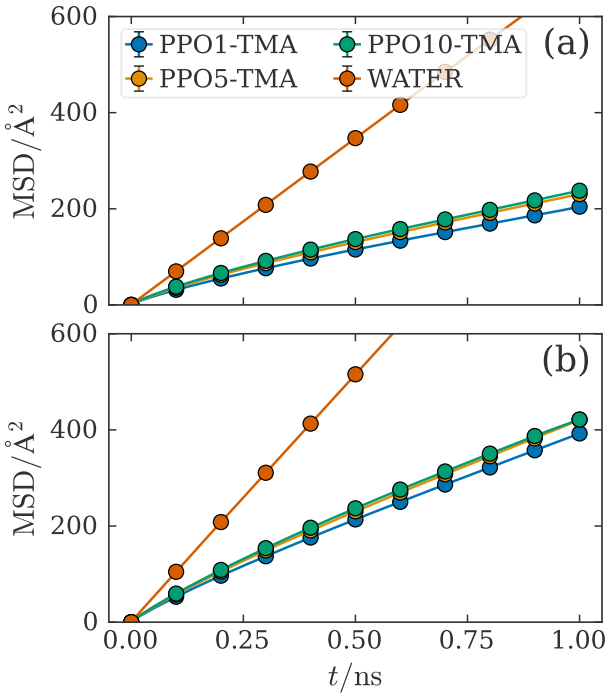

Figure 4: MSD of water molecules at $\lambda = 10$ (a) and $\lambda = 20$ (b) for PPO1-TMA, PPO5-TMA, PPO10-TMA membranes and free OH^-. If not visible, error bars are smaller than symbols.

can be seen on water and hydroxide molecules. At the hydration level ($\lambda = 10$), where the spacer length induces no differences in diffusive properties, there is still more than a factor 3 between the OH^- diffusion coefficient in KOH solution and in polymeric systems. We can make two assumptions from MSDs curves. On one hand, water diffusion properties are independent of the spacer length. What we found for perfluorosulfonated membranes[39] is verified for hydro-carbonated membranes. On the other hand, diffusion properties of hydroxide ions for PPO5-TMA and PPO10-TMA membranes are higher at the lower hydration level. As we discussed in the introduction, the diffusion of hydroxide ions takes place through two processes: the Grotthuss mechanism (where a proton defect hoppings from a water molecule to another) and a vehicular one, identical of water molecules diffusion. Grotthuss mechanism occurs along a hydrogen bond network, whose efficiency is strongly related to the connectivity of the hydrogen bonds network. Analyzing this network will provide meaningful informations about the reason why hydroxide ions diffuse faster in PPO5 and PPO10 TMA at low hydration state.

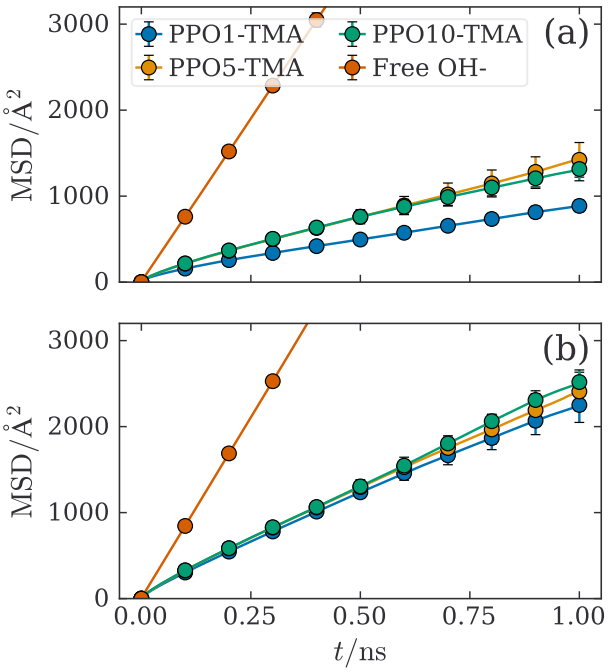

Figure 5: MSD of OH^- ions at $\lambda = 10$ (a) and $\lambda = 20$ (b) for PPO1-TMA, PPO5-TMA, PPO10-TMA membranes and free OH^-. If not visible, error bars are smaller than symbols.

In the case of non-confined systems and ideal solution, an hydroxide ion in its pseudo-Zundel form is connected to 4 hydrogen bonds with the surrounding water molecules (see Fig. 1 of Ref. 80). The analysis of these hydrogen bonds is critical to investigate the efficiency of the Grotthuss mechanism. How water molecules arrange around hydroxide ions is the first element to investigate. This is achieved by the means of radial distribution functions (RDFs) defined in Section 5 of the Supporting Information. RDFs and coordination numbers (CN) between oxygen of hydroxide ions (noted O*) and oxygen of water molecules (O) are plotted on Figure S2 of Supporting Information for all membranes at $\lambda = 10$ and 20. For comparison, are given the distribution functions of free OH^-. Whereas the impact of confinement is clearly established on the shape of the RDFs, the latter do not show a statistically-meaningful signature of an impact of the spacer length. Confining hydroxide ions

Table 2: Diffusion coefficients ($Å^2\,ps^{-1}$) of water and hydroxide anions in PPO1-TMA, PPO5-TMA and PPO10-TMA membranes and free OH^- at two λ hydration levels.

λ	D_{H_2O} ($Å^2\,ps^{-1}$)	D_{OH^-} ($Å^2\,ps^{-1}$)	$D_{OH^-}/D^{water}_{OH^-}$
		PPO1-TMA	
10	0.029	0.133	0.10
20	0.060	0.344	0.24
		PPO5-TMA	
10	0.033	0.220	0.17
20	0.063	0.380	0.27
		PPO10-TMA	
10	0.033	0.187	0.15
20	0.062	0.409	0.29
		Water	
10	0.113	1.279	1
20	0.173	1.416	1

strongly impacts their capacity to connect with surrounding water molecules. Quantifying the number of hydrogen bonds between hydroxide ions and water molecules should provide meaningful insights. Hydrogen bonds existence criteria were defined from the two-dimensional histogram plot represented on Figure S3 of the Supporting Information leading to a distance cutoff d_{O^*O} of 2.8 and an angle cutoff $\widehat{O^*HO}$ of 130°. Figure 6 shows the probability density of the number of hydrogen bonds per hydroxide ions at any hydration levels for all membranes and free OH^-. At $\lambda = 10$, distributions are disjointed, and the number of hydrogen bonds per hydroxide ions is slightly higher in the case of PPO5-TMA and PPO10-TMA membranes. This proves that hydroxide ions are closer to a bulk-like behaviour in PPO5/PPO10-TMA than in PPO1-TMA. At $\lambda = 20$, the differences vanish and distributions are identical, getting closer to that of free OH^-. As OH^- concentration decreases (i.e. λ increases), the distributions are shifted to the right, but are still below the value of 4. The influence of both concentration and confinement is then clearly established.

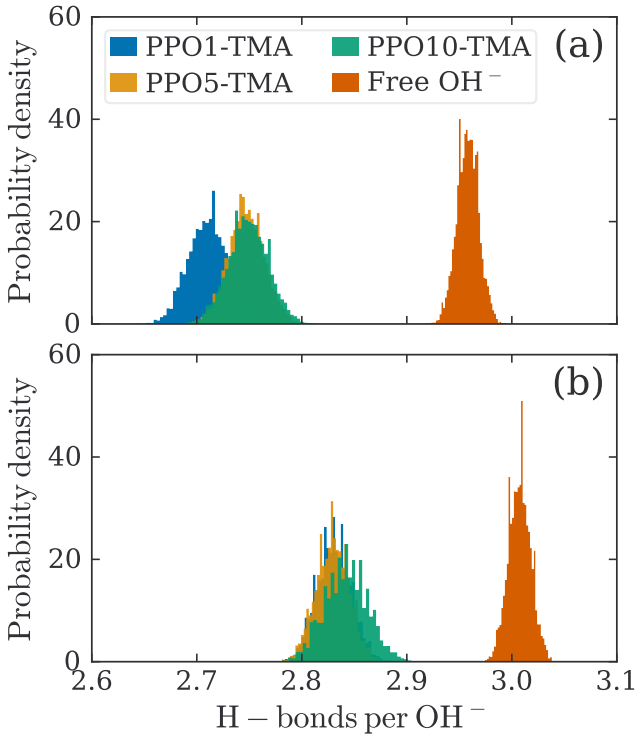

Figure 6: Probability density of the number of $H-$bonds per OH^- at $\lambda = 10$ (a) and $\lambda = 20$ (b) for PPO1-TMA and PPO5-TMA membranes.

We now focus on the efficiency of Grotthuss hoppings. Indeed, proton defects can jump back and forth from one water molecule to another. Such events are depicted as rattling in refs. 81–84. Without doing complex calculations to characterize such back and forth, counting the Grotthuss events and the number of unique visited oxygens of water phase by the proton defects provides meaningful insights. The results are collected in Table 3. At any hydration level, the numbers of Grotthuss events per picoseconds are the same within the standard deviations for all simulated membranes, and lower than free OH^-. This result confirms that the impact of the confinement on Grotthuss hoppings does not depend on the spacer length and that rattling is necessarily higher at low hydration state. This assumption is verified by investigating the number of unique

visited oxygens, which are higher at $\lambda = 20$ for all membranes. Moreover, at $\lambda = 10$, the number of visited oxygens is higher for PPO5-TMA and PPO10-TMA membranes, which is in agreement with the higher MSDs of PPO5-TMA and PPO10-TMA membranes at this hydration level. Number of unique visited oxygens is equal for all membranes at $\lambda = 20$. Interestingly, these results contradict those previously established which claim that the Grotthuss mechanism is predominant at high hydration.[85] We observe here that it is more a question of efficiency, driven by highly connected hydrogen bonds network, than predominance.

Table 3: Number of Grotthuss hoppings and unique visited oxygens for PPO1-TMA, PPO5-TMA, PPO10-TMA membranes and free OH^- at two hydration levels (λ).

λ	$n_{\text{Grotthuss hoppings}}$/ps	$n_{\text{visited oxygens}}$/ps
	PPO1-TMA	
10	876 ± 5	639 ± 3
20	882 ± 6	678 ± 3
	PPO5-TMA	
10	882 ± 4	647 ± 3
20	885 ± 5	681 ± 2
	PPO10-TMA	
10	879 ± 4	649 ± 2
20	890 ± 3	684 ± 2
	Free OH^-	
10	944 ± 1	706 ± 1
20	956 ± 1	738 ± 1

Questions remain as to the origin of the more tightly-connected hydrogen bonding network for PPO5-TMA and PPO10 membranes-TMA, and the threshold in spacer length. We will prove that the origin of this behaviour could arise from differences in spacer arrangements combined with the delocalization of OH^- ions with respect to the backbone. First, the pore size distributions are analysed. In the same way as our prior work,[39] a non-linear constraint optimization routine is used to locally compute, around each oxygen atom of the water phase, the largest inscribed sphere in the polymer host matrix. Pore size (d) distributions are represented on Figure 7.

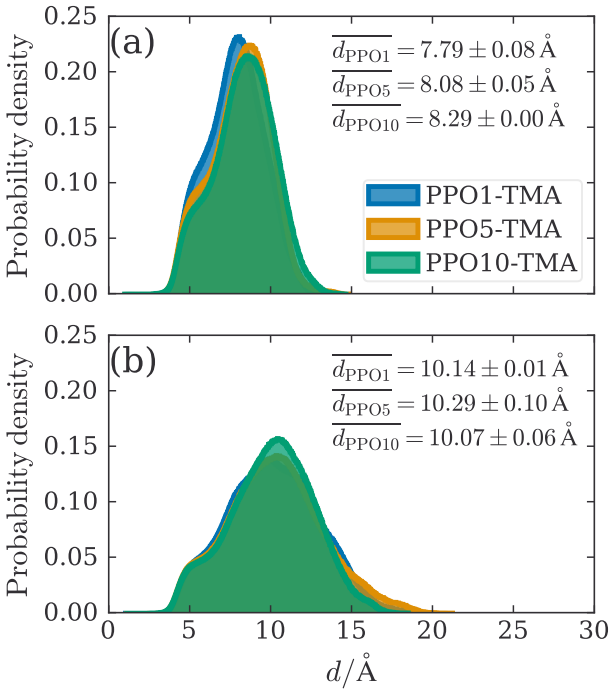

Figure 7: Pore size d distributions at $\lambda = 10$ (a) and $\lambda = 20$ (b). $\bar{d}$ are mean values.

Compared to perfluorosulfonic acid (PFSA) based membranes, PPO membranes obey to a different swelling law. Indeed, PFSA swells as the linear law[32,85,86] $d = \lambda$, whereas it is clearly not the case here. Moreover, we do not observe any heterogeneity in distributions, hence giving more uniform transport properties. Finally, diffusion properties and arrangement of hydrogen bond network are not shown to be related to the mean size of water domains in the membranes.

Then, to characterize spacer arrangements and OH^- delocalization, we compute pairwise distances between

- spacer carbon atoms and their first neighbour which is a carbon of backbone (see Figure 8) ;
- N of TMA^+ and their first neighbour which is a carbon of backbone (see Figure S4 of the Supporting Information) ;
- O^* and their first neighbour which is a carbon of backbone (see Figure S5 of the Supporting Information) ;

- O* and their first neighbour which is a carbon of spacer (see Figure S6 of the Supporting Information).

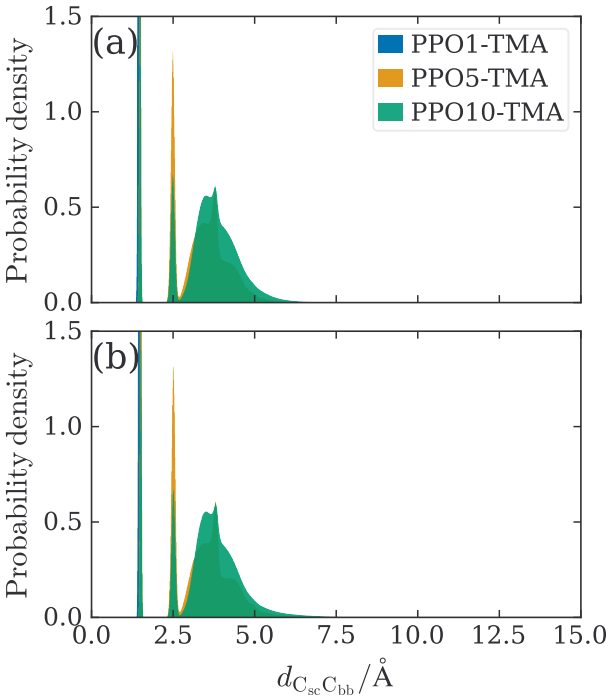

Figure 8: Probability density of pairwise distances between carbon atoms of spacers and the first nearest neighbors carbon atoms of backbones at $\lambda = 10$ (a) and $\lambda = 20$ (b).

For PPO1-TMA membranes, only one peak (located at approximately 1.4 Å) is present in Figure 8, as there is only one carbon atom in the spacer. For PPO5 and PPO10 membranes, the distributions are very similar. One might expect a greater flexibility for longer spacers, hence PPO10-TMA should exhibit a larger distribution. Nevertheless, because of hydrophobicity of spacers, the latter remains stuck on the backbones. Higher distances are present (up to 13 Å), but are still in the minority. The same behaviour can be observed between N atoms and C atoms of backbones (see Figure S4, zoomed in). Those distributions prove that the spacers effectively are aligned with the backbone. Increasing water content slightly increases spacer mobility, hence enlarged PPO5-TMA and PPO10-TMA distributions can be observed. With regard to the probability density of the distances between the O* atoms and the backbone carbons (see Figure S5), the longer the spacer, the further the OH^- ions are from the backbone. Especially at short distances, longest spacers screen the backbone. The associated behaviour for the distances between the O* atoms and the spacer carbons (see Figure S6) is that at short distances, carbon atoms of spacer form the local environment for OH^- ions. Highest distances correspond to delocalized OH^- ions in the water phase.

4 Conclusion

This work investigated the influence of spacer length on AEM structure/properties relationships using reactive molecular dynamics. Reactive molecular dynamics is a valuable method giving access to not only system of several thousands of atoms, like in non-reactive molecular dynamics, but also to reactivity. Indeed, reactive mechanisms in diffusion processes are of major importance in conductivity properties of membranes, which we want to be as high as possible. The first order parameter is unquestionably the water content. The higher it is, the more the membrane conducts. Many other parameters then drive the conduction properties, such as EWs, spacer steric hindrance, spacer length, cristallinity of membranes, tortuosity and conductivity of water channels. This makes these materials inherently multi-scale. Three AEM differing only in spacer length were simulated, namely PPO1-TMA (one carbon spacer), PPO5-TMA (five carbon spacer) and PPO10-TMA (ten carbons spacer). AEMs exhibit phase separation upon hydration: hydrophobic phase formed by PPO backbone, and hydrophilic phase formed by water and TMA groups. A more or less developed hydrogen bonds network emerges within the hydrophilic phase, depending on the spacer length and hydration state. The more the hydrogen bonds network is developed (in other word the more the hydroxide ions have a bulk-like behaviour), the more the hydroxide ions are free to diffuse through the membrane. A careful analysis of the hydrogen bonds network was provided in relation to the hydration level and

compared to free hydroxide ions in bulk water. The number of hydrogen bonds formed between OH^- and H_2O molecules is the key parameter to analyze in order to obtain informations about the diffusivity potential of OH^- ions. At the lower hydration level, membranes show differences in their diffusion properties: a longer spacer length implies higher diffusion properties. A threshold effect is nevertheless observed: PPO5-TMA and PPO10-TMA membranes show the same diffusion properties. Because of hydrophobicity of carbon spacers, the spacers remain rather stuck on the backbone, although pentyl and decyl spacers still have a certain flexibility with respect to PPO1-TMA, At high hydration state, there is enough water in the system to force diffusion properties to depend only on the polymer host matrix. Those results would mean that it exists, at a given hydration state, an optimal length for spacers, which also drives mechanical properties.[87] Moreover, short spacer length based membranes would have the highest potential to increase their transport properties as a function of hydration level. More specifically, this means that for a given level of hydration, there is an optimum spacer size due to hydrophobic interactions. On the other hand, the length of the spacer might drive (among other parameters) the equilibrium water uptake but the dependence between water uptake and spacer size does not allow a clear conclusion to be drawn. The water uptake of a membrane must therefore be calculated by molecular simulation, as it has been done in several recent studies.[88–90] However, we are convinced that these results are very important as they provide valuable insights for the design of AEMs with optimized properties. Future work should focus on exploring the proton counterpart, as hydrogen bonds between sulfonate groups and hydronium ions, which are typically used in proton exchange membranes, could complement the findings presented in this work.

Acknowledgement This work was performed in SimatLab, a joint public-private laboratory dedicated to the modeling of polymer materials. This laboratory is supported by Michelin, Clermont Auvergne University (UCA), CHU Clermont-Ferrand and CNRS. We are grateful to the Mésocentre Clermont Auvergne University for providing computing and storage resources. This work was performed using HPC resources from GENCI-IDRIS (Grant AD010913369).

Supporting Information Available

Protocol used to design the initial configurations for reactive MDs, distribution of water molecules around TMA^+ groups, operational expression for the calculation of mean square displacements, trajectories of reactive species, radial distribution functions, hydrogen bond criteria and pairwise distances.

References

(1) Bakangura, E.; Wu, L.; Ge, L.; Yang, Z.; Xu, T. Mixed Matrix Proton Exchange Membranes for Fuel Cells: State of The Art and Perspectives. *Prog. Polym. Sci.* **2016**, *57*, 103–152.

(2) Pan, Z.; An, L.; Zhao, T.; Tang, Z. Advances and Challenges in Alkaline Anion Exchange Membrane Fuel Cells. *Prog. Energy Combust. Sci.* **2018**, *66*, 141–175.

(3) Pollet, B. G.; Kocha, S. S.; Staffell, I. Current Status of Automotive Fuel Cells For Sustainable Transport. *Curr. Opin. Electrochem.* **2019**, *16*, 90–95.

(4) Steele, B. C.; Heinzel, A. Materials For Fuel-Cell Technologies. *Nature* **2001**, *414*, 345–352.

(5) Hren, M.; Božič, M.; Fakin, D.; Kleinschek, K. S.; Gorgieva, S. Alkaline Membrane Fuel Cells: Anion Exchange Membranes and Fuels. *Sustain. Energy Fuels* **2021**, *5*, 604–637.

(6) Jinnouchi, R.; Kudo, K.; Kodama, K.; Kitano, N.; Suzuki, T.; Minami, S.; Shinozaki, K.; Hasegawa, N.; Shinohara, A. The Role of Oxygen-Permeable Ionomer for Polymer Electrolyte Fuel Cells. *Nat. Commun.* **2021**, *12*, 4956.

(7) Zhang, H.; Shen, P. K. Recent Development of Polymer Electrolyte Membranes For Fuel Cells. *Chem. Rev.* **2012**, *112*, 2780–2832.

(8) Zhang, H.; Shen, P. K. Advances in the High Performance Polymer Electrolyte Membranes for Fuel Cells. *Chem. Soc. Rev.* **2012**, *41*, 2382–2394.

(9) Li, N.; Guiver, M. D.; Binder, W. H. Towards High Conductivity in Anion-Exchange Membranes For Alkaline Fuel Cells. *ChemSusChem* **2013**, *6*, 1376–1383.

(10) Zhang, H.-W.; Chen, D.-Z.; Xianze, Y.; Yin, S.-B. Anion-Exchange Membranes For Fuel Cells: Synthesis Strategies, Properties and Perspectives. *Fuel Cells* **2015**, *15*, 761–780.

(11) Karibayev, M.; Kalybekkyzy, S.; Wang, Y.; Mentbayeva, A. Molecular Modeling in Anion Exchange Membrane Research: A Brief Review of Recent Applications. *Molecules* **2022**, *27*, 3574.

(12) Ziv, N.; Mondal, A. N.; Weissbach, T.; Holdcroft, S.; Dekel, D. R. Effect of CO2 on the properties of anion exchange membranes for fuel cell applications. *J. Membr. Sci.* **2019**, *586*, 140–150.

(13) Duan, Q.; Ge, S.; Wang, C.-Y. Water Uptake, Ionic Conductivity and Swelling Properties of Anion-Exchange Membrane. *J. Power Sources* **2013**, *243*, 773–778.

(14) Tomasino, E.; Mukherjee, B.; Ataollahi, N.; Scardi, P. Water Uptake in an Anion Exchange Membrane Based on Polyamine: A First-Principles Study. *J. Phys. Chem. B* **2022**, *126*, 7418–7428.

(15) Du, N.; Roy, C.; Peach, R.; Turnbull, M.; Thiele, S.; Bock, C. Anion-Exchange Membrane Water Electrolyzers. *Chem. Rev.* **2022**, *122*, 11830–11895.

(16) You, W.; Noonan, K. J.; Coates, G. W. Alkaline-Stable Anion Exchange Membranes: A Review of Synthetic Approaches. *Prog. Polym. Sci.* **2020**, *100*, 101177.

(17) Chu, X.; Liu, J.; Miao, S.; Liu, L.; Huang, Y.; Tang, E.; Liu, S.; Xing, X.; Li, N. Crucial Role of Side-Chain Functionality in Anion Exchange Membranes: Properties and Alkaline Fuel Cell Performance. *J. Membr. Sci.* **2021**, *625*, 119172.

(18) Wang, Z.; Parrondo, J.; Ramani, V. Anion Exchange Membranes Based on Polystyrene-Block-Poly (Ethylene-Ran-Butylene)-Block-Polystyrene Triblock Copolymers: Cation Stability and Fuel Cell Performance. *J. Electrochem. Soc.* **2017**, *164*, F1216.

(19) Lin, X.; Liang, X.; Poynton, S. D.; Varcoe, J. R.; Ong, A. L.; Ran, J.; Li, Y.; Li, Q.; Xu, T. Novel Alkaline Anion Exchange Membranes Containing Pendant Benzimidazolium Groups For Alkaline Fuel Cells. *J. Membr. Sci* **2013**, *443*, 193–200.

(20) Wang, J.; Gu, S.; Kaspar, R. B.; Zhang, B.; Yan, Y. Stabilizing The Imidazolium Cation in Hydroxide-Exchange Membranes For Fuel Cells. *ChemSusChem* **2013**, *6*, 2079–2082.

(21) Guo, D.; Lai, A. N.; Lin, C. X.; Zhang, Q. G.; Zhu, A. M.; Liu, Q. L. Imidazolium-Functionalized Poly (Arylene Ether Sulfone) Anion-Exchange Membranes Densely Grafted With Flexible Side Chains For Fuel Cells. *ACS Appl. Mater. Int.* **2016**, *8*, 25279–25288.

(22) Li, Z.; Zhang, Y.; Cao, T.; Yang, Y.; Xiong, Y.; Xu, S.; Xu, Z. Highly Conductive Alkaline Anion Exchange Membrane

Containing Imidazolium-Functionalized Octaphenyl Polyhedral Oligomeric Silsesquioxane Filler. *J. Membr. Sci.* **2017**, *541*, 474–482.

(23) Ran, J.; Wu, L.; Ru, Y.; Hu, M.; Din, L.; Xu, T. Anion Exchange Membranes (AEMs) Based on Poly (2,6-Dimethyl-1,4-Phenylene Oxide)(PPO) and Its Derivatives. *Polym. Chem.* **2015**, *6*, 5809–5826.

(24) Dang, H.-S.; Weiber, E. A.; Jannasch, P. Poly (Phenylene Oxide) Functionalized With Quaternary Ammonium Groups Via Flexible Alkyl Spacers For High-Performance Anion Exchange Membranes. *J. Mat. Chem. A* **2015**, *3*, 5280–5284.

(25) Dang, H.-S.; Jannasch, P. Exploring Different Cationic Alkyl Side Chain Designs For Enhanced Alkaline Stability and Hydroxide Ion Conductivity of Anion-Exchange Membranes. *Macromolecules* **2015**, *48*, 5742–5751.

(26) Sung, S.; Mayadevi, T.; Min, K.; Lee, J.; Chae, J. E.; Kim, T.-H. Crosslinked PPO-based Anion Exchange membranes: The effect of Crystallinity Versus Hydrophilicity by Oxygen-Containing Crosslinker Chain Length. *J. Membr. Sci.* **2021**, *619*, 118774.

(27) Allen, M. P.; Tildesley, D. J. *Computer Simulation of Liquids*; Oxford: Clarendon Press, 1987.

(28) Zhang, W.; van Duin, A. C. T. ReaxFF Reactive Molecular Dynamics Simulation of Functionalized Poly(phenylene oxide) Anion Exchange Membrane. *J. Phys. Chem. C* **2015**, *119*, 27727–27736.

(29) Lee, M.-T.; Vishnyakov, A.; Neimark, A. V. Modeling Proton Dissociation and Transfer Using Dissipative Particle Dynamics Qimulation. *J. Chem. Theory Comput.* **2015**, *11*, 4395–4403.

(30) Lu, J.; Jacobson, L. C.; Perez Sirkin, Y. A.; Molinero, V. High-Resolution Coarse-Grained Model of Hydrated Anion-Exchange Membranes That Accounts For Hydrophobic and Ionic Interactions Through Short-Ranged Potentials. *J. Chem. Theory Comput.* **2017**, *13*, 245–264.

(31) Vanya, P.; Sharman, J.; Elliott, J. A. Mesoscale Simulations of Confined Nafion Thin Films. *J. Chem. Phys.* **2017**, *147*, 214904.

(32) Berrod, Q.; Hanot, S.; Guillermo, A.; Mossa, S.; Lyonnard, S. Water Sub-Diffusion in Membranes For Fuel Cells. *Sci. Rep.* **2017**, *7*, 8326.

(33) Vishnyakov, A.; Mao, R.; Lee, M.-T.; Neimark, A. V. Coarse-Grained Model of Nanoscale Segregation, Water Diffusion, and Proton Transport in Nafion Membranes. *J. Chem. Phys.* **2018**, *148*.

(34) Zhang, W.; van Duin, A. C. T. Improvement of the ReaxFF Description for Functionalized Hydrocarbon/Water Weak Interactions in the Condensed Phase. *J. Phys. Chem. B* **2018**, *122*, 4083–4092.

(35) Dong, D.; Zhang, W.; Barnett, A.; Lu, J.; Van Duin, A. C. T.; Molinero, V.; Bedrov, D. Multiscale Modeling of Structure, Transport and Reactivity in Alkaline Fuel Cell Membranes: Combined Coarse-Grained, Atomistic and Reactive Molecular Dynamics Simulations. *Polymers* **2018**, *10*, 1289.

(36) Dong, D.; Zhang, W.; Van Duin, A. C.; Bedrov, D. Grotthuss Versus Vehicular Transport of Hydroxide in Anion-Exchange Membranes: Insight From Combined Reactive and Nonreactive Molecular Simulations. *J. Phys. Chem. Lett.* **2018**, *9*, 825–829.

(37) Clark, J. A.; Santiso, E. E.; Frischknecht, A. L. Morphology and Proton Diffusion in a Coarse-Grained Model of Sulfonated Poly (Phenylenes). *J. Chem. Phys.* **2019**, *151*, 104901.

(38) Sen, U.; Ozdemir, M.; Erkartal, M.; Kaya, A. M.; Manda, A. A.; Oveisi, A. R.; Aboudzadeh, M. A.; Tokumasu, T. Mesoscale Morphologies of Nafion-Based Blend Membranes by Dissipative Particle Dynamics. *Processes* **2021**, *9*, 984.

(39) Flottat, T.; Latour, B.; Goujon, F.; Hauret, P.; Malfreyt, P. Investigating Percolation and Clustering Effects on Aquivion and Nafion Membranes at the Molecular Scale. *Int. J. Hydrogen Energy* **2023**, *48*, 33283–33296

(40) Hassanzadeh Afrouzi, H.; Moshfegh, A.; Farhadi, M.; Sedighi, K. Dissipative Particle Dynamics Simulation Hydrated Nafion EW 1200 as Fuel Cell Membrane in Nanoscopic S cale. *Chall. Nano Micro Scale Sci.* **2016**, *5*, 44–53.

(41) Ibergay, C.; Malfreyt, P.; Tildesley, D. J. Mesoscale Modeling of Polyelectrolyte Brushes With Salt. *J. Phys. Chem. B* **2010**, *114*, 7274–7285.

(42) Goujon, F.; Malfreyt, P.; Tildesley, D. J. Interactions Between Polymer Brushes and a Polymer Solution: Mesoscale Modelling of The Structural and Frictional Properties. *Soft Matter* **2010**, *6*, 3472–3481.

(43) Mabuchi, T.; Huang, S.-F.; Tokumasu, T. Nafion Ionomer Dispersion in Mixtures of 1-Propanol and Water Based on the Martini Coarse-Grained Model. *J. Polym. Sci.* **2020**, *58*, 487–499.

(44) Kreuer, K.-D.; Rabenau, A.; Weppner, W. Vehicle Mechanism, A New Model for the Interpretation of the Conductivity of Fast Proton Conductors. *Angewandte Chemie International Edition in English* **1982**, *21*, 208–209.

(45) Magnico, P. Molecular dynamics study on water and hydroxide transfer mechanisms in PSU-g-alkyl-TMA membranes at low hydration: Effect of side chain length. *Int. J. Hydrogen Energy* **2021**, *46*, 33915–33933.

(46) De Grotthuss, C. Memoir On The Decomposition of Water And Of The Bodies That It Holds In Solution By means Of Galvanic Electricity. *Biochim. Biophys. Acta Bioenerg.* **2006**, *1757*, 871–875.

(47) Iftimie, R.; Minary, P.; Tuckerman, M. E. Ab initio Molecular Dynamics: Concepts, Recent Developments, and Future Trends. *Proc. Natl. Acad. Sci. U.S.A.* **2005**, *102*, 6654–6659.

(48) Warshel, A.; Levitt, M. Theoretical Studies of Enzymic Reactions: Dielectric, Electrostatic and Steric Stabilization of The Carbonium Ion In The Reaction Of Lysozyme. *J. Mol. Biol.* **1976**, *103*, 227–249.

(49) Clemente, C. M.; Capece, L.; Martí, M. A. Best Practices on QM/MM Simulations of Biological Systems. *J. Chem. Inf. Model.* **2023**, *63*, 2609–2627.

(50) Phillpot, S. R.; Antony, A. C.; Shi, L.; Fullarton, M. L.; Liang, T.; Sinnott, S. B.; Zhang, Y.; Biner, S. B. Charge Optimized Many Body (COMB) potentials for simulation of nuclear fuel and clad. *Comput. Mater. Sci.* **2018**, *148*, 231–241.

(51) Jinnouchi, R.; Minami, S.; Karsai, F.; Verdi, C.; Kresse, G. Proton transport in perfluorinated ionomer simulated by machine-learned interatomic potential. *J. Phys. Chem. Lett.* **2023**, *14*, 3581–3588.

(52) Senftle, T. P.; Hong, S.; Islam, M. M.; Kylasa, S. B.; Zheng, Y.; Shin, Y. K.; Junkermeier, C.; Engel-Herbert, R.; Janik, M. J.; Aktulga, H. M. et al. The ReaxFF Reactive Force-Field: Development, Applications and Future Directions. *npj Comput. Mater.* **2016**, *2*, 1–14.

(53) Van Duin, A. C.; Dasgupta, S.; Lorant, F.; Goddard, W. A. ReaxFF: a Reactive Force Field For Fydrocarbons. *J. Phys. Chem. A* **2001**, *105*, 9396–9409.

(54) Chenoweth, K.; Van Duin, A. C.; Goddard, W. A. ReaxFF Reactive Force Field

for Molecular Dynamics Simulations of Hydrocarbon Oxidation. *J. Phys. Chem. A* **2008**, *112*, 1040–1053.

(55) Vashisth, A.; Ashraf, C.; Bakis, C. E.; van Duin, A. C. Effect of Chemical Structure on Thermo-Mechanical Properties of Epoxy Polymers: Comparison of Accelerated ReaxFF Simulations and Experiments. *Polymer* **2018**, *158*, 354–363.

(56) Vashisth, A.; Ashraf, C.; Zhang, W.; Bakis, C. E.; Van Duin, A. C. Accelerated ReaxFF Simulations for Describing The Reactive Cross-Linking Of Polymers. *J. Phys. Chem. A* **2018**, *122*, 6633–6642.

(57) Ashraf, C.; Vashisth, A.; Bakis, C. E.; Van Duin, A. C. Reactive Molecular Dynamics Simulations Of The Atomic Oxygen Impact On Epoxies With Different Chemistries. *J. Phys. Chem. C* **2019**, *123*, 15145–15156.

(58) Dasgupta, N.; Yilmaz, D. E.; Van Duin, A. Simulations Of The Biodegradation Of Citrate-Based Polymers For Artificial Scaffolds Using Accelerated Reactive Molecular Dynamics. *J. Phys. Chem. B* **2020**, *124*, 5311–5322.

(59) Gittus, O. R.; Bresme, F. Thermophysical Properties of Water Using Reactive Force Fields. *J. Chem. Phys.* **2021**, *155*, 114501.

(60) Karuth, A.; Alesadi, A.; Vashisth, A.; Xia, W.; Rasulev, B. Reactive Molecular Dynamics Study of Hygrothermal Degradation of Crosslinked Epoxy Polymers. *ACS Appl. Polym. Mater.* **2022**, *4*, 4411–4423.

(61) Stoppelman, J. P.; McDaniel, J. G. N-Heterocyclic Carbene Formation in the Ionic Liquid [EMIM$^+$][OAc$^-$]: Elucidating Solvation Effects with Reactive Molecular Dynamics Simulations. *J. Phys. Chem. B* **2023**, *127*, 5317–5333

(62) Zhang, W.; Van Duin, A. C. Second-Generation ReaxFF Water Force Field: Improvements in the Description of Water Density and OH-Anion Diffusion. *J. Phys. Chem. B* **2017**, *121*, 6021–6032.

(63) Fedkin, M. V.; Shin, Y. K.; Dasgupta, N.; Yeon, J.; Zhang, W.; Van Duin, D.; Van Duin, A. C.; Mori, K.; Fujiwara, A.; Machida, M. et al. Development Of The ReaxFF Methodology For Electrolyte–Water Systems. *J. Phys. Chem. A* **2019**, *123*, 2125–2141.

(64) Gomzi, V.; Sapic, I. M.; Vidak, A. ReaxFF Force Field Development and Application for Toluene Adsorption on MnMO x (M = Cu, Fe, Ni) Catalysts. *J. Phys. Chem. A* **2021**, *125*, 10649–10656.

(65) Dang, H.-S.; Jannasch, P. A comparative study of anion-exchange membranes tethered with different hetero-cycloaliphatic quaternary ammonium hydroxides. *J. Mater. Chem. A* **2017**, *5*, 21965–21978.

(66) MedeA-3.5, Materials Design, Inc., San Diego, CA, USA, 2022.

(67) Zhang, W.; Dong, D.; Bedrov, D.; van Duin, A. C. T. Hydroxide transport and chemical degradation in anion exchange membranes: a combined reactive and non-reactive molecular simulation study. *J. Mater. Chem. A* **2019**, *7*, 5442–5452.

(68) Nosé, S.; Klein, M. Constant Pressure Molecular Dynamics for Molecular Systems. *Mol. Phys.* **1983**, *50*, 1055–1076.

(69) Nosé, S. A Molecular Dynamics Method for Simulations In the Canonical Ensemble. *Mol. Phys.* **1984**, *52*, 255–268.

(70) Eastwood, J. W.; Hockney, R. W.; Lawrence, D. N. P3M3DP - the 3-Dimensional Periodic Particle-Particle-Particle-Mesh Program. *Comput. Phys. Chem.* **1980**, *19*, 215–261.

(71) Thompson, A. P.; Aktulga, H. M.; Berger, R.; Bolintineanu, D. S.; Brown, W. M.; Crozier, P. S.; in 't Veld, P. J.; Kohlmeyer, A.; Moore, S. G.; Nguyen, T. D. et al. LAMMPS - a flexible

simulation tool for particle-based materials modeling at the atomic, meso, and continuum scales. *Comp. Phys. Comm.* **2022**, *271*, 108171.

(72) Gilois, B.; Goujon, F.; Fleury, A.; Soldera, A.; Ghoufi, A. Water nano-diffusion through the Nafion fuel cell membrane. *J. Membr. Sci.* **2020**, *602*, 117958.

(73) Hofmann, D.; Fritz, L.; Ulbrich, J.; Schepers, C.; Böhning, M. Detailed-atomistic molecular modeling of small molecule diffusion and solution processes in polymeric membrane materials. *Macromol Theory Simul* **2000**, *9*, 293–327.

(74) Ryckaert, J.-P.; Ciccotti, G.; Berendsen, H. J. Numerical integration of the cartesian equations of motion of a system with constraints: molecular dynamics of n-alkanes. *J. Comput. Phys.* **1977**, *23*, 327–341.

(75) Monti, S.; Corozzi, A.; Fristrup, P.; Joshi, K. L.; Shin, Y. K.; Oelschlaeger, P.; Van Duin, A. C.; Barone, V. Exploring The Conformational And Reactive Dynamics Of Biomolecules In Solution Using An Extended Version Of The Glycine Reactive Force Field. *Phys. Chem. Chem. Phys.* **2013**, *15*, 15062–15077.

(76) te Velde, G.; Bickelhaupt, F. M.; Baerends, E. J.; Fonseca Guerra, C.; van Gisbergen, S. J. A.; Snijders, J. G.; Ziegler, T. Chemistry with ADF. *J. Comput. Chem.* **2001**, *22*, 931–967.

(77) de Vos Burchart, E.; Verheij, V.; Van Bekkum, H.; Van de Graaf, B. A Consistent Molecular Mechanics Force Field For All-Silica Zeolites. *Zeolites* **1992**, *12*, 183–189.

(78) Furman, D.; Wales, D. J. Transforming the Accuracy and Numerical Stability of ReaxFF Reactive Force Fields. *J. Phys. Chem. Lett.* **2019**, *10*, 7215–7223.

(79) Foglia, F.; Berrod, Q.; Clancy, A. J.; Smith, K.; Gebel, G.; Sakai, V. G.; Appel, M.; Zanotti, J.-M.; Tyagi, M.; Mahmoudi, N. et al. Disentangling water, ion and polymer dynamics in an anion exchange membrane. *Nat. Mater.* **2022**, *21*, 555–563.

(80) Tuckerman, M. E.; Marx, D.; Parrinello, M. The nature and transport mechanism of hydrated hydroxide ions in aqueous solution. *Nature* **2002**, *417*, 925–929.

(81) Tuckerman, M. E.; Marx, D.; Parrinello, M. The Nature And Transport Mechanism Of Hydrated Hydroxide Ions In Aqueous Qolution. *Nature* **2002**, *417*, 925–929.

(82) Tuckerman, M. E.; Chandra, A.; Marx, D. Structure and Dynamics Of OH-(aq). *Acc. Chem. Res.* **2006**, *39*, 151–158.

(83) Marx, D.; Chandra, A.; Tuckerman, M. E. Aqueous Basic Solutions: Hydroxide Solvation, Structural Diffusion, And Comparison To The Hydrated Proton. *Chem. Rev.* **2010**, *110*, 2174–2216.

(84) Ma, Z.; Tuckerman, M. E. On The Connection Between Proton Transport, Structural Diffusion, And Reorientation Of The Hydrated Hydroxide Ion As A Function Of Temperature. *Chem. Phys. Lett.* **2011**, *511*, 177–182.

(85) Kusoglu, A.; Weber, A. Z. New Insights into Perfluorinated Sulfonic-Acid Ionomers. *Chem. Rev.* **2017**, *117*, 987–1104.

(86) Berrod, Q.; Lyonnard, S.; Guillermo, A.; Ollivier, J.; Frick, B.; Manseri, A.; Améduri, B.; Gébel, G. Nanostructure and Transport Properties of Proton Conducting Self-Assembled Perfluorinated Surfactants: A Bottom-Up Approach toward PFSA Fuel Cell Membranes. *Macromolecules* **2015**, *48*, 6166–6176.

(87) Kreuer, K.; Schuster, M.; Obliers, B.; Diat, O.; Traub, U.; Fuchs, A.; Klock, U.; Paddison, S.; Maier, J. Short-side-chain proton conducting perfluorosulfonic acid ionomers: Why they perform better in PEM fuel cells. *J. Power Sources* **2008**, *178*, 499–509.

(88) Kali, R.; Milner, S. T. Simulations predict water uptake and transport in nanostructured ion exchange membranes. *J. Membr. Sci.* **2023**, *687*, 122060.

(89) Sireci, E.; De Luca, G.; Luque Di Salvo, J.; Cipollina, A.; Micale, G. Prediction of equilibrium water uptake and ions diffusivities in ion-exchange membranes combining molecular dynamics and analytical models. *J. Membr. Sci.* **2023**, *668*, 121283.

(90) Luque Di Salvo, J.; De Luca, G.; Cipollina, A.; Micale, G. Effect of ion exchange capacity and water uptake on hydroxide transport in PSU-TMA membranes: A DFT and molecular dynamics study. *J. Membr. Sci.* **2020**, *599*, 117837.

TOC Graphic